Electronic structure of MnO and CoO from the B3LYP hybrid density functional method

Xiaobing Feng
Department of Physics, Dalian Railway Institute, Dalian 116028, People's Republic of China
(Received 26 July 2003; revised manuscript received 4 December 2003; published 15 April 2004)

The electronic and magnetic properties of CoO and MnO have been studied with the B3LYP hybrid density functional method. The ground states have been correctly predicted by the B3LYP functional, and it gives better results for energy gaps, magnetic moments, and core-level binding energies than the generalized gradient approximation (GGA) and the unrestricted Hartree-Fock (UHF) method. The B3LYP results for energy gaps, magnetic moments and core-level binding energies are between the GGA and UHF ones for antiferromagnetic, ferromagnetic and nonmagnetic phases of MnO and CoO. Although the two materials have same structure and antiferromagnetic ordering, the electronic structures near the Fermi energies are different. The magnetic coupling constants of CoO are much larger than the ones of MnO. The hyperfine coupling constants and electric field gradients are also calculated for further comparisons with experiment.

DOI: 10.1103/PhysRevB.69.155107 PACS number(s): 71.20.Be, 71.15.Mb, 71.27.+a

I. INTRODUCTION

Transition metal oxides (TMOs) are prototypes of Mott insulators.[1] The metal-insulator transitions, through high pressures, chemical doping, and increasing temperatures, are an old and still challenging research subject.[2,3] The discovery of high temperature superconductivity in cuprate materials containing CuO_2 planes has further activated interest in these systems. Similar to TMOs the parent compounds of high temperature superconductors are antiferromagnetic insulators at low temperatures; they become superconducting after hole dopings. Because of the strong Coulomb repulsion between the two $3d$ electrons on the transition metal ions these systems show some specific properties that are not well described within the well-known local density approximation (LDA) or generalized gradient approximation (GGA) of the density functional theory. The conventional energy band calculations based on the LDA and GGA failed to predict the correct ground states for some of these strongly correlated electronic systems (SCESs), especially in the insulating phases, such as FeO, CoO, $CaCuO_2$, La_2CuO_4, etc.[4] For some other TMOs the energy gaps are severely underestimated, e.g., NiO. The failures of the LDA and GGA result from the unphysical self-interaction between an electron with itself, which is inherent in the LDA and GGA energy functionals. The self-interaction is not important in common metals, because the quasiparticles are itinerant. In materials with localized orbitals, such as $3d$ or $4f$ orbitals, the self-interaction tends to delocalize the $3d$ or $4f$ electrons, which results in wrong predictions for some of the electronic properties of the SCESs. The self-interaction corrected (SIC) LDA did recover the correct ground states of some SCESs.[5,6] The LDA$+U$ method also succeeded in predicting the correct ground states.[7] LDA$+U$ does not subtract the self-interaction from the energy functional; rather it introduces an additional interaction, which is missed due to the self-interaction, between two electrons on the same localized orbitals. The simple unrestricted Hartree-Fock (UHF) approximation was also able to predict the correct ground states for the strongly correlated antiferromagnetic insulators due to the lack of self-interaction, although the energy gaps and magnetic moments are always overestimated.[8]

Recently, the B3LYP hybrid density functional method,[9,10] which is well known in the study of thermochemistry of atoms and molecules, has been applied to some periodic systems.[11–15] In B3LYP the nonlocal Hartree-Fock exchange has been mixed into the GGA exchange-correlation energy, and the weight coefficients have been determined by fitting the thermochemical experimental data of some atoms and molecules. The applications to periodic systems show that B3LYP significantly improves energy gaps and magnetic moments for some materials with antiferromagnetic insulating ground states, such as NiO,[11,12,14] CoO,[11] MnO,[12] La_2CuO_4,[13] and $CaCuO_2$.[15] In addition, B3LYP gives rather accurate energy gaps for some semiconductors,[12] which is a significant improvement over LDA results. It has been well known that LDA gives energy gaps of semiconductors underestimated over 30%. The self-interaction is not important for common semiconductors, the improvements are due to the better description for the correlation energy in B3LYP. SIC-LDA and LDA$+U$ are not expected to improve much on the theoretical energy gaps for semiconductors.

The application of B3LYP to La_2CuO_4 shows that the band structure is in agreement with the SIC-LSD and LDA $+U$ schemes, with the energy gap being in better agreement with experiment. It is also pointed out that the contribution to the doped hole from the Cu d_{z^2} may not be negligible for high temperature superconductors.[13] For $CaCuO_2$, it is clearly seen that the energy band crossing the Fermi level separated to form an insulating gap;[15] the mechanism is quite similar to LDA$+U$, though no semiempirical Hubbard U was introduced. The magnetic coupling constants are also in good agreement with the experiment. The effects of Hartree exchange on the electronic, magnetic, and structural properties of NiO has been studied.[11] It is asserted that 35% of Hartree exchange admixed into the LDA functional could provide better results for magnetic coupling constants than the original hybrid density functional.[14] But the energy gap is about 50% larger than the B3LYP and the experimental results.

In this paper we study the electronic structures of MnO and CoO with the B3LYP method. We keep the original

weight coefficients and treat the functional as a parameter-free one. MnO and CoO crystallize in the rock-salt structure. Their ground states are type-II antiferromagnetic (AFII) insulators, with ferromagnetic (111) planes and alternating spins in neighboring planes. Below the Néel temperatures, 118 K for MnO and 292 K for CoO, there are slight rhombohedral distortions along the [111] direction. MnO has largest magnetic moments among the transition metal monoxides, with five parallel *d*-electron spins. The ground state of CoO can be correctly predicted by B3LYP, while the LDA failed to generate an antiferromagnetic insulator. In previous B3LYP calculations on CoO the theoretical lattice constant, energy gap, magnetic moment, heat of atomization and Fermi energy are reported.[11] Here, we calculate the magnetic coupling constants, core-level energies, electric field gradients, and hyperfine coupling constants. In addition, a detailed electronic structure of CoO is calculated, while only the total densities of states of Co and O are reported in Ref. 11. This paper is focused on the electronic and magnetic properties of the two materials. The B3LYP results show significant improvements over GGA and UHF.

II. FORMULA AND CALCULATION METHOD

In the hybrid functional scheme the nonlocal Hartree-Fock (HF) approach is mixed into the energy functional of the GGA. The argument for mixing the HF exchange into the exchange-correlation energy is based on the adiabatic connection formula.[9] The weights for the gradient-corrected correlation energy, local exchange energy, and exact HF exchange terms were determined by a linear least-square fitting of the thermochemical properties of some atoms and molecules to the experiments. The atom with highest atomic number used in the fitting is Cl. No atoms with *d* or higher shells were used. 20% of the exact HF exchange energy in the exchange-correlation energy gives theoretical results in good agreement with experiments. In the so-called B3LYP scheme the Perdew-Wang[16] gradient-corrected correlation energy, which was used in the original work of Becke,[9] is replaced by Lee-Yang-Parr correlation energy.[10]

The final exchange-correlation energy functional reads[9]

$$E_{XC}=(1-a_0)E_X^{LSDA}+a_0E_X^{exact}+a_X\Delta E_X^{B88}+E_C^{LSDA}+a_C\Delta E_C^{LYP}, \quad (1)$$

in which the local spin density approximation (LSDA) of Vosko, Wilk, and Nusair[17] is used for E_X^{LSDA} and E_C^{LSDA}. E_X^{exact} is the exact nonlocal HF exchange energy. ΔE^{B88} and ΔE_C^{LYP} are the Becke's[18] and Lee-Yang-Parr's gradient corrections for the local exchange and correlation energies, respectively. The optimum values for the parameters a_0, a_X, and a_C are 0.20, 0.72, and 0.81, respectively.[9]

The admixture of HF exchange has important effects on the electronic and magnetic properties of materials, especially for correlated electronic systems. It is realized that the success of B3LYP results from the removal of the self-interaction due to the introduction of HF exchange, but the mechanism is not very clear. The removal of self-interaction is not enough to get better results for highly correlated systems; a better correlation energy is also essential to take the dynamical correlation effects into account. The UHF method usually obtains energy gaps well over 10 eV, which is several times larger than the experimental energy gaps. To obtain the correct energy gaps many-body screening effects on the Coulomb interaction from the dynamical correlation must be appropriately incorporated into the density functionals. This is an effective way to obtain a better correlation energy by fitting to experimental results. It is expected that a special set of weight coefficients optimized for a specific class of materials with the same structure and electronic characters could generate better results. In this paper, we retain the original coefficients and take it as a parameter-free functional.

The calculations are carried out with CRYSTAL package.[19] The basis vectors for expanding the Kohn-Sham orbitals are Bloch functions composed of localized contracted Gaussian basis sets.[20] All-electron basis sets for Mn and Co ions are of the form of 86-411(41*d*)*G*, the basis set for oxygen ion is of the form of 8-411*G*. The real-space mesh technique was used to calculate the integrals involving the local exchange and correlation potentials, which could reduce the numerical errors introduced by fitting the potentials with Gaussian functions.

In the calculations 65 points in the irreducible part of the first Brillouin zone were used. We adopt 7, 7, 7, 7, and 14 as the integral tolerances to obtain high precision in monoelectronic and bielectronic integrals. The convergence threshold exponents are set as 7 and 7. A supercell has been built to take the antiferromagnetic order into account. For comparisons, UHF and GGA calculations were also carried out with the same basis sets and precisions.

III. RESULTS AND DISCUSSION

Figure 1 gives the curves of the total energy versus lattice parameter for MnO and CoO. The nonmagnetic, ferromagnetic (FM), type-I antiferromagnetic (AFI) and AFII states have been studied with the B3LYP functional. In the AFI state there are ferromagnetic (001) planes and alternating spins in neighboring planes. From Fig. 1 the equilibrium lattice parameters are obtained. One can see that the B3LYP functional can correctly predict the ground states for MnO and CoO, with the magnetic states having the lower energies and larger lattice parameters than the nonmagnetic state. The strong on-site Coulomb repulsion favors moment formation on transition metal ions, leading to magnetic states having lower energies than the nonmagnetic state. The energy differences between the magnetic states for MnO is much smaller than the ones for CoO, and this is in agreement with the experimental results that CoO has a higher magnetic transition temperature than MnO.

The magnetic coupling constants between the nearest magnetic moments (J_1) and the next nearest moments (J_2) can be extracted from the total energies of different magnetic phases. On neglecting the transverse fluctuations of the Heisenberg Hamiltonian one can get a generalized Ising model

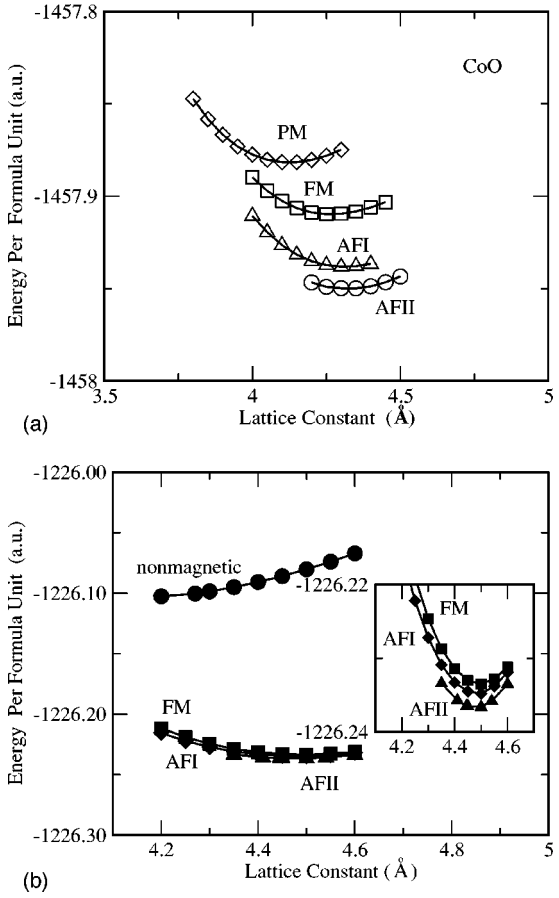

FIG. 1. The total energies vs lattice parameters for CoO (a) and MnO (b). Calculations are carried out for nonmagnetic, ferromagnetic (FM), type-I (AFI), and type-II (AFII) antiferromagnetic phases. The inset in (b) shows an enlargement of the curves near the equilibrium lattice parameter.

$$H = J_1 \sum_{NN} S_{iz} S_{jz} + J_2 \sum_{NNN} S_{iz} S_{jz}, \qquad (2)$$

in which only magnetic couplings between the nearest neighbors (NNs) and next nearest neighbors (NNNs) are taken into account. It is shown that in some cases the mapping between the Ising model and the Heisenberg model justifies the evaluation of magnetic coupling constants with the Ising model.[21–24] The magnetic coupling constants can be written as $J_1 = (E_{FM} - E_{AFI})/8S^2$ and $J_2 = [2J_1 + (E_{AFI} - E_{AFII})/S^2]/6$,[25] where E_{FM}, E_{AFI}, and E_{AFII} represent the total energies of ferromagnetic and type-I, and type-II antiferromagnetic phases. The spin S for MnO and CoO are taken as $\frac{5}{2}$ and $\frac{3}{2}$, respectively. One can obtain $J_1 = 9.80$ K and $J_2 = 20.5$ K for MnO, $J_1 = 486$ K and $J_2 = 439$ K for CoO. The J_1 of MnO is same as the one obtained with the linear augmented planewave (LAPW) LDA,[25] and J_2 is a little smaller than the LDA result. Other LDA calculations reported larger J_1 and J_2 for MnO.[26,27] Due to the large energy differences between different magnetic phases of CoO J_1 and J_2 of CoO are much larger than that of MnO. For some transition metal oxides, such as CoO and FeO, the LDA could not predict the correct ground states, magnetic coupling constants could not be extracted with the LDA.

TABLE I. The energy gaps (Δ, in eV), magnetic moments (m, in μ_B) and lattice constants (a, in Å) of CoO and MnO from GGA, UHF, and B3LYP approaches. The experimental lattice parameters of MnO and CoO are used in the calculations for energy gaps and magnetic moments. AFII, AFI, FM, and NM denote type-II, type-I, ferromagnetic, and nonmagnetic phases, respectively.

	GGA	UHF	B3LYP	Expt.
Δ (CoO, AFII)	0	4.84	3.63	2.4 (Ref. 28)
m (CoO, AFII)	2.46	2.91	2.69	3.35 (Ref. 29), 3.8 (Ref. 30), 3.98 (Ref. 31)
a (CoO, AFII)			4.317	4.254 (Ref. 32)
Δ (CoO, AFI)	0	13.5	1.14	
m (CoO, AFI)	2.07	2.89	2.74	
Δ (CoO, FM)	0	0	0	
m (CoO, FM)	2.38	2.85	2.69	
Δ (CoO, NM)	0	0	0	
Δ (MnO, AFII)	1.28	13.3	3.92	3.6–3.8 (Ref. 33), 3.98 (Ref. 34)
m (MnO, AFII)	4.55	4.91	4.73	4.58 (Ref. 35), 4.79 (Ref. 36)
a (MnO, AFII)			4.495	4.4448 (Ref. 37)
Δ (MnO, AFI)	0	12.3	2.70	
m (MnO, AFI)	4.56	4.92	4.75	
Δ (MnO, FM)	0	11.9	1.89	
m (MnO, FM)	4.47	4.91	4.78	
Δ (MnO, NM)	0	10.1	0	

For the AFII phase, which is the ground state of MnO and CoO, the theoretical energy gaps, magnetic moments and the equilibrium lattice constants from GGA, UHF, and B3LYP approaches are given in Table I. For MnO the magnetic moment and the energy gap are in good agreement with experiments. For the two materials the B3LYP results are between the GGA and UHF results. The difference between the B3LYP magnetic moment and the experimental values results from the orbital moment. In our calculations the magnetic moments come from spin densities; the orbital moments are not taken into account. For CoO the orbital moment is estimated at about $(0.66–1.29)\mu_B$. The orbital moment, $1.28\mu_B$, can be deduced from the B3LYP spin moment and the experimental orbital-to-spin angular moment ratio of $L/S = 0.95$.[38] The B3LYP lattice constants for MnO and CoO are a little larger than the experimental results, this is also the case for other materials, e.g., $CaCuO_2$.[15] The previous B3LYP results for the energy gap, 3.5 eV, and lattice constant, 4.29 Å, are a little less than the ones reported here, although the previous magnetic moment is in agreement with the present one.[11] The reason for this may be due to the different techniques used for calculating the integrals in the local exchange and correlation potentials. In the present calculations the real space mesh technique is used to eliminate the errors caused by the incompleteness of the auxiliary basis sets, which are used for fitting the local exchange and correlation potentials. In addition, the energy gap reported in Ref.

TABLE II. The core-level binding energies (in eV) of O 1*s*, Co 2*p* and Mn 2*p* of CoO and MnO from GGA, UHF, and B3LYP approaches. The experimental results for CoO and MnO are taken from Ref. 28 and Ref. 39, respectively. Experimental lattice parameters are used in the calculations.

	GGA	UHF	B3LYP	Expt.
O 1*s* (CoO)	508.6	554.9	517.5	529.4
Co 2*p* (CoO)	762.5	816.9	773.8	779.8
O 1*s* (MnO)	508.0	554.6	517.2	529.7
Mn 2*p* (MnO)	623.1	670.0	633.0	641.0

11 is obtained with a theoretical equilibrium lattice parameter, while the energy gap in Table I is obtained with the experimental lattice parameter.

For CoO insulating states can be obtained with UHF and B3LYP for AFI and AFII magnetic orderings. The UHF method predicts that the total energy of AFI state is 3.65 eV per chemical formula unit lower than AFII state. It means that the ground state of CoO is not correctly predicted by the UHF approach. The GGA failed to generate insulating states for all the three kinds of magnetic states and the nonmagnetic state. The spin magnetic moment is also underestimated by the GGA. For MnO the UHF approach predicts that all the four kinds of phases are insulating, while B3LYP predicts that nonmagnetic state is metallic. GGA generated an energy gap only for AFII phase. The LAPW-LDA calculation also showed that only AFII ordering is predicted to be insulating.[25] The three theoretical approaches all predict that the spin magnetic moment does not change much for difference magnetic phases, with the B3LYP results being between the GGA and UHF ones.

In Table II the core-level binding energies of O 1*s*, Co 2*p* and Mn 2*p* are compared with experiments.[28,39] The theoretical results shown in Table II are calculated in the AFII phases. Our calculations also show that the core-level binding energies are nearly same for AFII and nonmagnetic phases. Both the theoretical and experimental results for O 1*s* show that O 1*s* has nearly the same binding energies in the two materials, indicating that the core-level binding energies are not sensitive to the chemical environments in transition metal monoxides. From Table II one can see that the B3LYP results are also between the GGA and UHF ones, and the B3LYP results are in better agreements with the experiments. The overestimation of the binding energies by the UHF method comes from the insufficient screenings of the Coulomb interactions.

The band structures of CoO from the B3LYP and GGA approaches are shown in Fig. 2. It is interesting to see how the admixture of HF exchange turns the metal, which is the ground state of the GGA, into an insulator. The partial wave densities of states (DOSs) of CoO from the B3LYP and GGA approaches are shown in Fig. 3. One can see from Figs. 2 and 3 that the HF exchange does not change the dispersion of the bands very much, but the flat bands composed mainly of Co e_g and t_{2g} orbitals have been raised well above the Fermi energy. The highest occupied band, mainly composed of Co t_{2g} orbital, has been separated from the rest of the valence

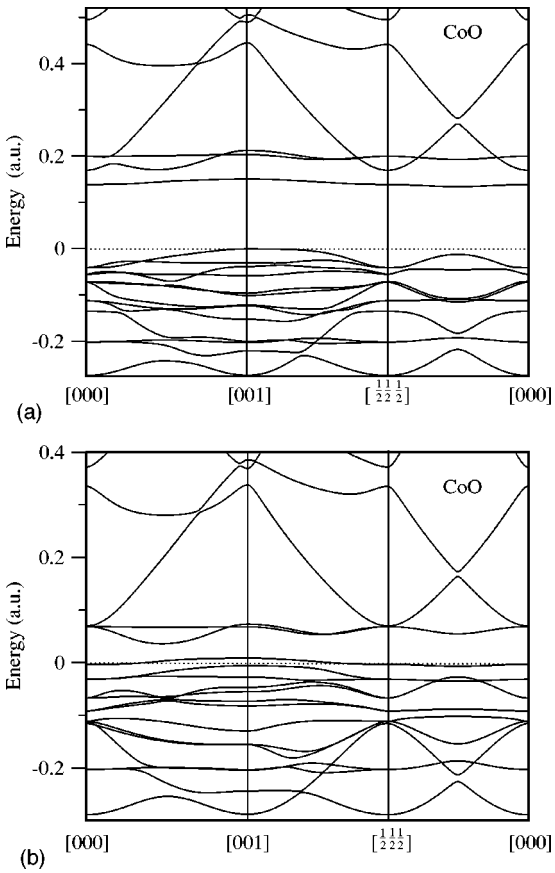

FIG. 2. The energy dispersions of CoO along high symmetry lines in the AFII phase from B3LYP (a) and GGA (b). For an insulating state the top of the valence band is taken as the reference energy.

bands. This mechanism of gap formation in CoO results from the strong Coulomb interaction between two 3*d* electrons. The GGA could not take the Coulomb interaction properly into account due to the self-interaction in the GGA energy functional.

The B3LYP and GGA DOSs of MnO are shown in Fig. 4. One can see that the mixing of nonlocal HF exchange caused the unoccupied bands move 2.64 eV further away from the valence bands. Although the GGA gave a energy gap of 1.28 eV, it is significantly smaller that the experimental value. MnO and CoO have the same structure and ground state magnetic ordering, but the electronic structures of the two systems are quite different. From Fig. 4(a) one can see that the highest occupied valence bands of MnO are composed of Mn e_g and O *p* orbitals, and the lowest unoccupied bands are mainly from Mn t_{2g} orbital. Figure 3(a) shows that Co t_{2g} and O *p* orbitals are responsible for the top of the valence bands, and the lowest unoccupied band results from the narrow band from Co t_{2g} orbital. The difference of the electronic structures of the two materials results mainly from the different numbers of *d* electrons on Mn and Co ions. Compared with the Mn ion, the Co ion has two additional 3*d* electrons, which occupy the Co t_{2g} orbitals. Due to this difference the main component of the highest occupied valence band changed from Mn e_g in MnO to Co t_{2g} in CoO. The

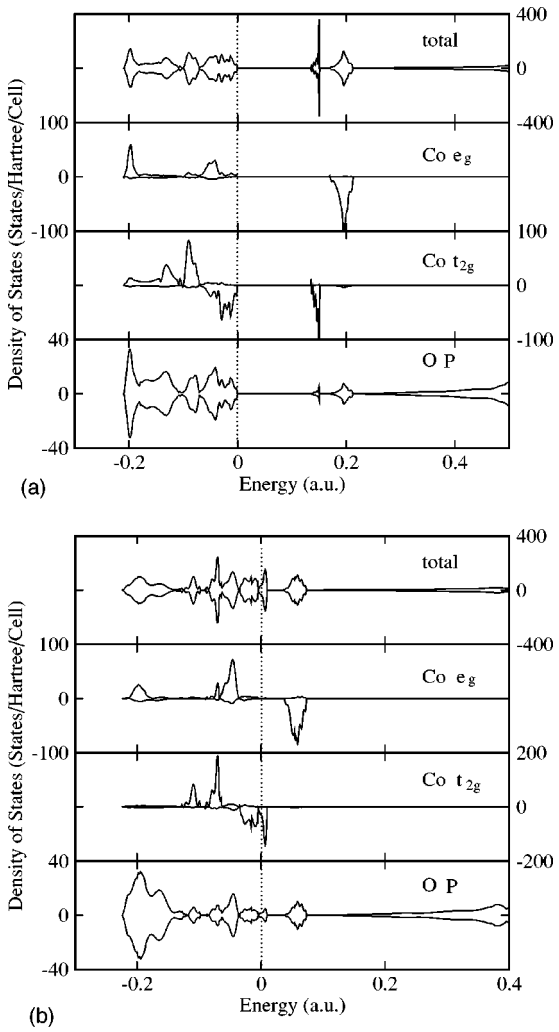

FIG. 3. The projected densities of states (DOS) of the Co $3d$ and O p partial waves from B3LYP (a) and GGA (b). The spin-up ion is chosen for the Co $3d$ DOS. The positive and negative DOSs represent the spin-up and spin-down DOSs, respectively. For an insulating state the top of the valence band is taken as the reference energy.

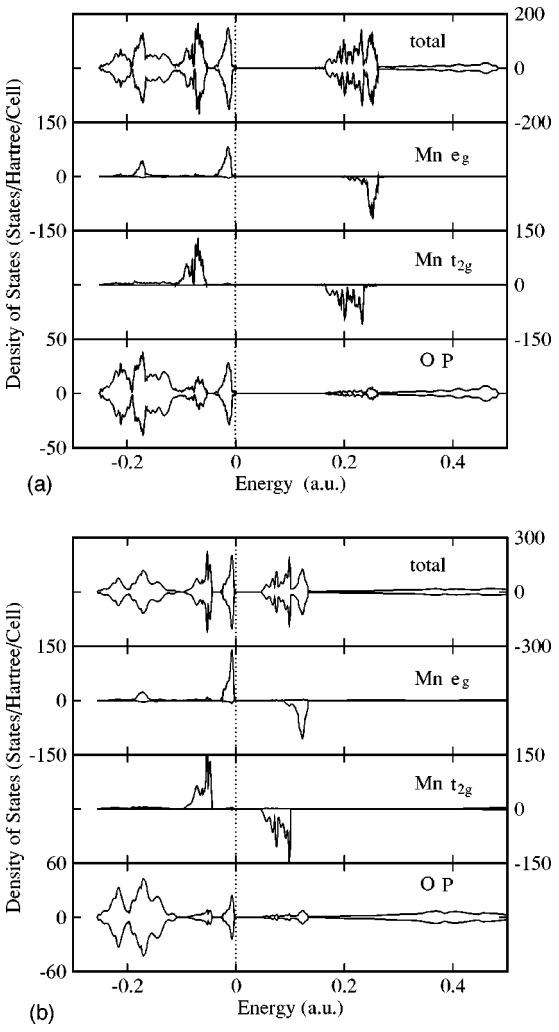

FIG. 4. The projected DOSs of the Mn $3d$ and O p partial waves from B3LYP (a) and GGA (b) schemes. The positive and negative DOSs represent the spin-up and spin-down DOSs, respectively. The top of the valence band is taken as the reference energy.

difference in the electronic structures is at the origin of significantly different magnetic coupling constants of the two materials.

There are significant contribution of O $2p$ states at the top of the valence bands. This is in agreement with the photoemission spectroscopy and the cluster model analyses[40] that MnO is close to the boundary between the Mott-Hubbard and charge transfer regimes in the Zaanen-Sawatzky-Allen classification scheme.[41] But, because TMOs are highly correlated systems, the rigid band model does not apply to TMOs. One could not know from the calculation on an undoped system how a doped hole would be distributed among the partial waves. A reliable way to analyze the hole composition is to do calculations on the system with one hole.

The nuclear magnetic resonance (NMR) is a powerful tool to explore the spin dynamics of materials. The nuclear quadruple resonance (NQR) frequency is determined by the electric field gradients (EFG) at the nuclear positions. To see the effect of the mixing of HF exchange into the energy functional the maximum components of the EFG tensors in the principal axis system and the hyperfine coupling constants have been calculated with GGA, UHF, and B3LYP

TABLE III. The maximum components of the traceless electric field gradient (EFG) tensors and hyperfine coupling constants (a_n) of MnO and CoO in AFII phase. The EFG is in the atomic unit and a_n in MHz. Experimental lattice parameters are used.

	GGA	UHF	B3LYP
EFG (Co)	1.01	-1.41	1.17
EFG (O)	0.110	-0.0256	0.150
a_n (Co)	117	558	200
a_n (O)	1.39×10^{-6}	1.04×10^{-6}	0.42
EFG (Mn)	0.00123	-0.00223	0.00467
EFG (O)	0.0244	0.00142	0.0123
a_n (Mn)	92.9	936	250
a_n (O)	4.74×10^{-6}	2.13×10^{-4}	1.28

approaches for CoO and MnO. One can see from Table III that the B3LYP results of hyperfine coupling constants a_n for oxygens in CoO and MnO are much larger than the ones from the GGA and UHF approaches. For EFGs and the a_n for Co and Mn the B3LYP results are closer to the GGA results than the UHF ones. The large a_n from the UHF method for Co and Mn are due to the large magnetic moments of the UHF approach.

IV. CONCLUSION

The electronic and magnetic properties of CoO and MnO have been studied with the B3LYP hybrid density functional. The results for energy gaps, magnetic moments, and core-level binding energies show that the B3LYP improves significantly over GGA and UHF approaches. Energy gaps and spin magnetic moments from B3LYP are in good agreement with experiment. Both GGA and UHF approaches failed to predict the correct ground state of CoO. The calculations on MnO and CoO show that for all the phases (the type-I, type-II, ferromagnetic, and nonmagnetic phases) the B3LYP results for energy gaps, magnetic moments, and core-level binding energies are between the GGA and UHF results. In agreement with experiment the O $1s$ core-level energies in MnO and CoO have nearly the same values. The B3LYP results for O $1s$, Co $2p$, and Mn $2p$ core levels are a little smaller that the experimental ones, with the largest relative error being about 2% for O $1s$. Due to the different numbers of $3d$ electrons of Co and Mn ions the electronic structure of CoO near the Fermi energy is different from that of MnO. The magnetic coupling constants of CoO are more than 20 times larger than the ones of MnO; the difference is due to the different electronic structures of the two materials. B3LYP predicts that the hyperfine coupling constants at oxygen sites in MnO and CoO are significantly larger than the ones obtained with GGA and UHF approaches. For the maximum components of the traceless electric field gradients tensors of the two materials the B3LYP results are more close to the GGA results than the UHF ones.

ACKNOWLEDGMENT

The author is grateful to Professor N. M. Harrison for enlightening discussions on transition metal oxides.

[1] N. F. Mott, *Metal-Insulator Transitions* (Taylor & Francis, London, 1990).
[2] R.E. Cohen, I.I. Mazin, and D.G. Isaak, Science **275**, 654 (1997).
[3] M. Imada, A. Fujimori, and Y. Tokura, Rev. Mod. Phys. **70**, 1039 (1998).
[4] W.E. Pickett, Rev. Mod. Phys. **61**, 433 (1989).
[5] A. Svane and O. Gunnarsson, Phys. Rev. Lett. **65**, 1148 (1990).
[6] D. Singh, W.E. Pickett, and H. Krakauer, Physica C **162-164**, 1431 (1989).
[7] V.I. Anisimov, J. Zaanen, and O.K. Andersen, Phys. Rev. B **44**, 943 (1991).
[8] See for example, M.D. Towler, N.L. Allan, N.M. Harrison, V.R. Saunders, W.C. Mackrodt, and E. Apra, Phys. Rev. B **50**, 5041 (1994).
[9] A.D. Becke, J. Chem. Phys. **98**, 5648 (1993).
[10] C. Lee, W. Yang, and R.G. Parr, Phys. Rev. B **37**, 785 (1988).
[11] T. Bredow and A.R. Gerson, Phys. Rev. B **61**, 5194 (2000).
[12] J. Muscat, A. Wander, and N.M. Harrison, Chem. Phys. Lett. **342**, 397 (2001).
[13] J.K. Perry, J. Tahir-Kheli, and W.A. Goddard, Phys. Rev. B **63**, 144510 (2001).
[14] I.P.R. Moreira, F. Illas, and R.L. Martin, Phys. Rev. B **65**, 155102 (2002).
[15] X. B. Feng and N. M. Harrison, http://arxiv.org/abs/cond-mat/0212588.
[16] J. P. Perdew, in *Electronic Structure of Solids*, edited by P. Ziesche and H. Eschrig (Academic Press, Verlag, Berlin, 1991).
[17] S.H. Vosko, L. Wilk, and M. Nusair, Can. J. Phys. **58**, 1200 (1980).
[18] A.D. Becke, Phys. Rev. A **38**, 3098 (1988).
[19] V. R. Saunders, R. Dovesi, C. Roetti, M. Causa, N. M. Harrison, R. Orlando, and C. M. Zicovich-Wilson, *CRYSTAL98 User's Manual* (University of Torino, Torino, 1998).
[20] http://www.chimifm.unito.it/teorica/crystal/Basis_Sets/mendel.html
[21] I.P.R. Moreira and F. Illas, Phys. Rev. B **55**, 4129 (1997).
[22] P. Reinhardt, M.P. Habas, R. Dovesi, I. de P.R. Moreira, and F. Illas, Phys. Rev. B **59**, 1016 (1999).
[23] Y.-S. Su, T.A. Kaplan, S.D. Mahanti, and J.F. Harrison, Phys. Rev. B **59**, 10521 (1999).
[24] D. Dai and M.-H. Whangbo, J. Chem. Phys. **118**, 29 (2003); **114**, 2887 (2001).
[25] J.E. Pask, D.J. Singh, I.I. Mazin, C.S. Hellberg, and J. Kortus, Phys. Rev. B **64**, 024403 (2001).
[26] T. Oguchi, K. Terakura, and A.R. Williams, Phys. Rev. B **28**, 6443 (1983); J. Appl. Phys. **55**, 2318 (1984).
[27] I.V. Solovyev and K. Terakura, Phys. Rev. B **58**, 15 496 (1998).
[28] J. van Elp, J.L. Wieland, H. Eskes, P. Kuiper, G.A. Sawatzky, F.M.F. de Groot, and T.S. Turner, Phys. Rev. B **44**, 6090 (1991).
[29] D.C. Khan and R.A. Erickson, Phys. Rev. B **1**, 2243 (1970).
[30] W.L. Roth, Phys. Rev. **110**, 1333 (1958).
[31] W. Jauch, M. Reehuis, H.J. Bleif, F. Kubanek, and P. Pattison, Phys. Rev. B **64**, 052102 (2001).
[32] M.J. Carey, F.E. Spada, A.E. Berkowitz, W. Cao, and G. Thomas, J. Mater. Res. **6**, 2680 (1991).
[33] R.N. Iskenderov, I.A. Drabkin, L.T. Emel'yanova, and Ya.M. Ksendzov, Fiz. Tverd. Tela (Leningrad) **10**, 2573 (1968) [Sov. Phys. Solid State **10**, 2031 (1969)].
[34] J. van Elp, R.H. Potze, H. Eskes, R. Berger, and G.A. Sawatzky, Phys. Rev. B **44**, 1530 (1991).
[35] A.K. Cheetham and D.A.O. Hope, Phys. Rev. B **27**, 6964 (1983).
[36] B.E.F. Fender, A.J. Jacobson, and F.A. Wegwood, J. Chem. Phys. **48**, 990 (1968).
[37] R. W. G. Wyckoff, *Crystal Structures* (Interscience, New York, 1964).
[38] W. Neubeck, C. Vettier, F. de Bergevin, F. Yakhou, D. Mannix, L.

Ranno, and T. Chatterji, J. Phys. Chem. Solids **62**, 2173 (2001).
[39] J. van Elp, R.H. Potze, H. Eskes, R. Berger, and G.A. Sawatzky, Phys. Rev. B **44**, 1530 (1991).
[40] A. Fujimori, N. Kimizuka, T. Akahane, T. Chiba, S. Kimura, F. Minami, K. Siratori, M. Taniguchi, S. Ogawa, and S. Suga, Phys. Rev. **42**, 7580 (1990).
[41] J. Zaanen, G.A. Sawatzky, and J.W. Allen, Phys. Rev. Lett. **55**, 418 (1985).